

Network Diffusions via Neural Mean-Field Dynamics

Shushan He *

Hongyuan Zha †

Xiaoqing Ye ‡

Abstract

We propose a novel learning framework based on neural mean-field dynamics for inference and estimation problems of diffusion on networks. Our new framework is derived from the Mori-Zwanzig formalism to obtain an exact evolution of the node infection probabilities, which renders a delay differential equation with memory integral approximated by learnable time convolution operators, resulting in a highly structured and interpretable RNN. Directly using cascade data, our framework can jointly learn the structure of the diffusion network and the evolution of infection probabilities, which are cornerstone to important downstream applications such as influence maximization. Connections between parameter learning and optimal control are also established. Empirical study shows that our approach is versatile and robust to variations of the underlying diffusion network models, and significantly outperform existing approaches in accuracy and efficiency on both synthetic and real-world data.

1 Introduction

Continuous-time information diffusion on networks is a prevalent phenomenon [5, 48, 51]. News spreading on social media [16, 19, 58], viral marketing [26, 28, 60], computer malware propagation, and epidemics of contagious diseases [4, 43, 51, 55] are all examples of diffusion on networks, among many others. For instance, a piece of information (such as a tweet) can be retweeted by users (nodes) with followee-follower relationships (edge) on the Twitter network. We call a user *infected* if she retweets, and her followers see her retweet and can also become infected if they retweet in turn, and so on. Such information diffusion mimics the epidemic spread where an infectious virus can spread to individuals (human, animal, or plant) and then to many others upon their close contact.

In this paper, we are mainly concerned with the estimation of individual node infection probabilities as well as inference of the underlying diffusion network structures directly using cascade data of past diffusion events on the network. For infection probability estimation, we want to compute the evolution of the probability of each node being infected during a diffusion initiated from a set of source nodes. For network structure inference, we aim at learning the edges as well as the strength of interactions between nodes through the edges on the network. Not surprisingly, both problems are very challenging, due to the extremely large scale of modern networks, the heterogeneous inter-dependencies among the nodes, and the randomness exhibited in cascade data.

Summary of Contributions We propose a novel learning framework, called neural mean-field (NMF) dynamics, to tackle both of the estimation and inference problems mentioned above. The main contribution of this paper consists of four parts: (i) We develop a neural mean-field dynamics framework to model the evolution of diffusion on a network. Our new framework is derived from the Mori-Zwanzig formalism to obtain an *exact* time evolution of the node infection probability with dimension linear in the network size; (ii) We show that the memory term of the Mori-Zwanzig equation can be approximated by a trainable convolution network, which renders the dynamical system into a delay differential equation. We show, for the first time, that the time discretization of such system reduces to a recurrent neural network. The approximate system is highly *interpretable*, and in particular, the training accepts sample cascades as input,

*Department of Mathematics and Statistics, Georgia State University, Atlanta, GA 30303, USA. Email: she4@gsu.edu.

†School of Computational Science and Engineering, Georgia Institute of Technology, North Avenue, Atlanta, GA 30332, USA. Email: zha@cc.gatech.edu.

‡Department of Mathematics and Statistics, Georgia State University, Atlanta, GA 30303, USA. Email: xye@gsu.edu.

and returns both individual probability estimates (and hence the influence function) as well as structure information of the diffusion network as outputs; (iii) We show that the parameters learning in NMF can be reduced to an optimal control problem with the parameters as time invariant control inputs, maximizing the *total Hamiltonian* of the system; and (iv) Our empirical analysis shows that our approach is robust to the variation of the unknown underlying diffusion models, and it also significantly outperforms existing approaches for both synthetic and real-world diffusion networks.

Notations We use boldfaced lower (upper) letter to denote vector (matrix) or vector-valued (matrix-valued) function, and $(\cdot)_k$ (or $(\cdot)_{ij}$) for its k th component (or (i, j) -th entry). All vectors are column vectors by default. We use $[\mathbf{x}; \mathbf{y}]$ to denote the vector that stacks \mathbf{x} and \mathbf{y} vertically, and $\mathbf{x} \cdot \mathbf{y}$ for the inner product. Time is denoted by t in either continuous ($t \in [0, T]$) or discrete case ($t = 0, 1, \dots, T$) for some time horizon $T \in \mathbb{R}_+$ (\mathbb{N} in discrete case). Derivative $'$ is with respect to t , and gradient $\nabla_{\mathbf{x}}$ is with respect to \mathbf{x} . Probability is denoted by $\Pr(\cdot)$, and expectation with respect to X (or p_X) is denoted by $\mathbb{E}_X[\cdot]$.

Paper outline In Section 2, we introduce the diffusion network models and related background information, including the influence predication and structure inference problems. In Section 3, we develop the proposed framework of neural mean-field dynamics for inference and prediction on diffusion networks, as well as an optimal control formulation for parameter learning. We demonstrate the performance of the proposed method on influence estimation and maximization on a variety of synthetic and real-world networks in Section 4. An overview of related work in the literature is provided in Section 5. Section 6 concludes the paper.

2 Preliminaries on Diffusion Networks

Diffusion network models Consider a diffusion network model, which consists of a network $\mathcal{G} = (\mathcal{V}, \mathcal{E})$ with node set $\mathcal{V} = [n] := \{1, \dots, n\}$ and (directed) edge set $\mathcal{E} \subset \mathcal{V} \times \mathcal{V}$, and a *diffusion model* that describes the distribution $p(t; \alpha_{ij})$ of the time t node i takes to infect a healthy neighbor $j \in \{j' : (i, j') \in \mathcal{E}\}$ for every $(i, j) \in \mathcal{E}$. Then, given a source (seed) set \mathcal{S} of nodes that are infected at time 0, they will infect their healthy neighbors with infection time following p , and the infected neighbors will then infect their healthy neighbors, and so on, such that the infection initiated from \mathcal{S} at time 0 propagates to other nodes of the network.

Typical diffusion network models are assumed to be *progressive* where infected node cannot recover and the infections on different edges are independent. For example, the standard diffusion model with exponential distribution $p(t; \alpha) = \alpha e^{-\alpha t}$ is mostly widely used; other distributions can also be considered, as is done in this paper. For simplicity, we focus on uni-parameter distributions or distributions with multiple parameters but only one can vary across different edges with the consequence that the parameter $\alpha_{ij} \geq 0$ indicates the *strength* of impact node i has on j .

Cascade data Observation data \mathcal{D} of a diffusion network are often in the form of *sample cascades* $\mathcal{D} := \{\mathcal{C}_k = (\mathcal{S}_k, \boldsymbol{\tau}_k) \in \mathcal{V} \times \mathbb{R}_+^n : k \in [K]\}$, where the k th cascade \mathcal{C}_k records its source set \mathcal{S}_k and the time $(\boldsymbol{\tau}_k)_i > 0$ indicates when node i was infected (if i was not infected during \mathcal{C}_k then $(\boldsymbol{\tau}_k)_i = \infty$). We also equate \mathcal{C}_k with $\{\hat{\mathbf{x}}^{(k)}(t) \in \{0, 1\}^n : i \in [n], t \geq 0\}$ such that $(\hat{\mathbf{x}}^{(k)}(t))_i = 1$ if the node i is infected at time t and 0 otherwise. For example, $\hat{\mathbf{x}}^{(k)}(0) = \boldsymbol{\chi}_{\mathcal{S}_k}$ where $(\boldsymbol{\chi}_{\mathcal{S}_k})_i = 1$ if $i \in \mathcal{S}_k$ and 0 otherwise. Such cascade data are collected from historical events for training purposes.

Prediction and inference Given the network $\mathcal{G} = (\mathcal{V}, \mathcal{E})$, as well as the diffusion model and \mathbf{A} , where $(\mathbf{A})_{ij} = \alpha_{ij}$ is the parameter of $p(t; \alpha_{ij})$ for edge (i, j) , the Inference *prediction* is to compute

$$\mathbf{x}(t; \boldsymbol{\chi}_{\mathcal{S}}) = [x_1(t; \boldsymbol{\chi}_{\mathcal{S}}), \dots, x_n(t; \boldsymbol{\chi}_{\mathcal{S}})]^\top \in [0, 1]^n \quad (1)$$

for any time $t > 0$ and any source set $\mathcal{S} \subset \mathcal{V}$. In (1), $x_i(t; \boldsymbol{\chi}_{\mathcal{S}})$ is the probability of node i being infected at time t given \mathcal{S} (not necessarily observed as a source set in \mathcal{D}). Note that we use $\boldsymbol{\chi}_{\mathcal{S}}$ and \mathcal{S} interchangeably hereafter. The probability $\mathbf{x}(t; \boldsymbol{\chi}_{\mathcal{S}})$ can also be used to compute the *influence* function $\sigma(t; \mathcal{S}) := \mathbf{1}_n^\top \mathbf{x}(t; \boldsymbol{\chi}_{\mathcal{S}})$,

the expected number of infected nodes at time t . Note that an analytic solution of (1) is intractable due to the exponentially large state space of the complete dynamical system of the diffusion problem [23, 57].

On the other hand, network *inference* refers to learning the network connectivity \mathcal{E} and \mathbf{A} given cascade data \mathcal{D} . The matrix \mathbf{A} is the distribution parameters if the diffusion model p is given, or it simply qualitatively measures the strength of impact node i on j if no specific p is known.

Influence prediction may also require the estimation of $\mathbf{x}(t; \chi_{\mathcal{S}})$ when only cascade data \mathcal{D} are available. This can be tackled by a *two-stage* approach, where a network inference is performed first to learn the network structure \mathcal{E} and the diffusion model parameters \mathbf{A} , and then an influence estimation is used to compute the influence for the source set \mathcal{S} . However, approximation errors and biases in the two stages will certainly accumulate. Alternately, one can use a *one-stage* approach to directly estimate $\mathbf{x}(t; \chi_{\mathcal{S}})$ of any \mathcal{S} from the cascade data \mathcal{D} , which is more versatile and less prone to diffusion model misspecification. Our method is a such kind of one-stage method. Additionally, it allows knowledge of \mathcal{E} and/or \mathbf{A} , if available, be integrated in order to improve performance.

Influence maximization Given cascade data \mathcal{D} , *influence maximization* is to find the source set \mathcal{S} that generates the maximal influence $\sigma(t; \mathcal{S})$ at t among all subsets of size n_0 , where $t > 0$ and $1 \leq n_0 < n$ are prescribed. Namely, influence maximization can be formulated as

$$\max_{\mathcal{S}} \sigma(t; \mathcal{S}), \quad \text{s.t.} \quad \mathcal{S} \subset \mathcal{V}, \quad |\mathcal{S}| \leq n_0. \quad (2)$$

There are two main ingredients of an influence maximization method for solving (2): an influence prediction subroutine that evaluates the influence $\sigma(t; \mathcal{S})$ for any given source set \mathcal{S} , and an (approximate) combinatorial optimization solver to find the optimal set \mathcal{S} of (2) that repeatedly calls the subroutine. The combinatorial optimization problem is NP-hard and is often approximately solved by greedy algorithms with guaranteed sub-optimality when $\sigma(t; \mathcal{S})$ is submodular in \mathcal{S} . In our experiment, we show that a greedy approach equipped with our proposed influence estimation method outperforms other state-of-the-art influence maximization algorithms.

3 Neural Mean-Field Dynamics

3.1 Mean-field Dynamics of Diffusion

Modelling diffusion by stochastic jump processes We begin with the jump process formulation of network diffusion. Given a source set $\chi_{\mathcal{S}}$, let $X_i(t; \chi_{\mathcal{S}})$ denote the infection status of the node i at time t . Namely, $X_i(t) = 1$ if node i is infected by time t , and 0 otherwise. Then $\{X_i(t) : i \in [n]\}$ are a set of n coupled jump processes, such that $X_i(t; \chi_{\mathcal{S}})$ jumps from 0 to 1 when the node i is infected at t . Let $\lambda_i^*(t)$ be the conditional intensity of $X_i(t; \chi_{\mathcal{S}})$ given history $\mathcal{H}(t) = \{X_i(s; \chi_{\mathcal{S}}) : s \leq t, i \in [n]\}$, i.e.,

$$\lambda_i^*(t) := \lim_{\tau \rightarrow 0^+} \frac{\mathbb{E}[X_i(t + \tau; \chi_{\mathcal{S}}) - X_i(t; \chi_{\mathcal{S}}) | \mathcal{H}(t)]}{\tau}. \quad (3)$$

Note that the numerator of (3) is also the conditional probability $\Pr(X_i(t + \tau) = 1, X_i(t) = 0 | \mathcal{H}(t))$ for any $\tau > 0$. In influence prediction, our goal is to compute the probability $\mathbf{x}(t; \chi_{\mathcal{S}}) = [x_i(t; \chi_{\mathcal{S}})]$ in (1), which is the expectation of $X_i(t; \chi_{\mathcal{S}})$ conditioning on $\mathcal{H}(t)$:

$$x_i(t; \chi_{\mathcal{S}}) = \mathbb{E}_{\mathcal{H}(t)}[X_i(t; \chi_{\mathcal{S}}) | \mathcal{H}(t)]. \quad (4)$$

To this end, we adopt the following notations (for simplicity we temporarily drop $\chi_{\mathcal{S}}$ in this subsection as the source set \mathcal{S} is arbitrary but fixed):

$$x_I(t) = \mathbb{E}_{\mathcal{H}(t)}[\prod_{i \in I} X_i(t; \chi_{\mathcal{S}}) | \mathcal{H}(t)], \quad y_I(t) = \prod_{i \in I} x_i(t), \quad e_I(t) = x_I(t) - y_I(t) \quad (5)$$

for all $I \subset [n]$ and $|I| \geq 2$. Then we can derive the evolution of $\mathbf{z} := [\mathbf{x}; \mathbf{e}]$ as follows.

Theorem 1. *The evolution of $\mathbf{z}(t) = [\mathbf{x}(t); \mathbf{e}(t)]$ follows the nonlinear differential equation:*

$$\mathbf{z}' = \bar{\mathbf{f}}(\mathbf{z}), \quad \text{where} \quad \bar{\mathbf{f}}(\mathbf{z}) = \bar{\mathbf{f}}(\mathbf{x}, \mathbf{e}) = [\mathbf{f}(\mathbf{x}; \mathbf{A}) - (\mathbf{A} \odot \mathbf{E})\mathbf{1}; \dots, f_I(\mathbf{x}, \mathbf{e}); \dots], \quad (6)$$

with initial value $\mathbf{z}_0 = [\chi_S; \mathbf{0}]$, $\mathbf{E} = [e_{ij}] \in \mathbb{R}^{n \times n}$, and

$$\mathbf{f}(\mathbf{x}; \mathbf{A}) = \mathbf{A}\mathbf{x} - \text{diag}(\mathbf{x})\mathbf{A}\mathbf{x}, \quad (7)$$

$$f_I(\mathbf{x}, \mathbf{e}) = \sum_{i \in I} \sum_{j \notin I} \alpha_{ji} (y_I - y_{I \cup \{j\}} - e_I + e_{I \cup \{j\}}) - \sum_{i \in I} y_{I \setminus \{i\}} \sum_{j \neq i} \alpha_{ji} (x_j - y_{ij} - e_{ij}). \quad (8)$$

Proof is provided in Appendix A. Here $\mathbf{x}(t) \in [0, 1]^n$ is the *resolved* variable whose value is of interests and samples can be observed in cascade data \mathcal{D} , and $\mathbf{e}(t) = [\dots, e_I(t), \dots] \in \mathbb{R}^{N-n}$ is the *unresolved* variable. The evolution (6) holds exactly for the standard diffusion model, but also approximately well for other distributions p , as shown in our empirical study. In either case, the dimension of \mathbf{z} is $N = 2^n - 1$, which is intractable computationally when n is large. To overcome this issue, we employ the Mori-Zwanzig formalism [9] to derive a reduce-order model of \mathbf{x} only.

Mori-Zwanzig memory closure We employ the Mori-Zwanzig (MZ) formalism [9] that allows to introduce a generalized Langevin equation (GLE) of the \mathbf{x} part of the dynamics. The GLE of \mathbf{x} is derived from the original equation (6) describing the evolution of $\mathbf{z} = [\mathbf{x}; \mathbf{e}]$, while maintaining the effect of the unresolved part \mathbf{e} . This is particularly useful in our case, as we only need \mathbf{x} for infection probability and influence estimation.

Define the Liouville operator \mathcal{L} such that $\mathcal{L}[g](\mathbf{z}) := \bar{\mathbf{f}}(\mathbf{z}) \cdot \nabla_{\mathbf{z}} g(\mathbf{z})$ for any real-valued function g of \mathbf{z} . Let $e^{t\mathcal{L}}$ be the Koopman operator associated with \mathcal{L} such that $e^{t\mathcal{L}}g(\mathbf{z}(0)) = g(\mathbf{z}(t))$ where $\mathbf{z}(t)$ solves (6). Then \mathcal{L} is known to satisfy the semi-group property for all g , i.e., $e^{t\mathcal{L}}g(\mathbf{z}) = g(e^{t\mathcal{L}}\mathbf{z})$. Now consider the projection operator \mathcal{P} as the truncation such that $(\mathcal{P}g)(\mathbf{z}) = (\mathcal{P}g)(\mathbf{x}, \mathbf{e}) = g(\mathbf{x}, 0)$ for any $\mathbf{z} = (\mathbf{x}, \mathbf{e})$, and its orthogonal complement as $\mathcal{Q} = I - \mathcal{P}$ where I is the identity operator. The following theorem describes the *exact* evolution of $\mathbf{x}(t)$, and the proof is given in Appendix A.

Theorem 2. *The evolution of \mathbf{x} specified in (6) can also be described by the following GLE*

$$\mathbf{x}' = \mathbf{f}(\mathbf{x}; \mathbf{A}) + \int_0^t \mathbf{k}(t-s, \mathbf{x}(s)) \, ds, \quad (9)$$

where \mathbf{f} is given in (7), and $\mathbf{k}(t, \mathbf{x}) := \mathcal{P}\mathcal{L}e^{t\mathcal{Q}\mathcal{L}}\mathcal{Q}\mathcal{L}\mathbf{x}$.

Note that, (9) is *not* an approximation—it is an *exact* representation of the \mathbf{x} part of the original problem (6). The equation (9) can be interpreted as a *mean-field* equation, where the two terms on the right hand side are called the *streaming term* (corresponding to the mean-field dynamics) and *memory term*, respectively. The mean-field dynamics provide the *main drift* of the evolution, and the memory term in a convolution form is for vital *adjustment*. This inspires us to approximate the memory term as a time convolution on \mathbf{x} , which naturally yields a delay differential equation and further reduces to a recurrent neural network (RNN) in discretization, as shown in the next subsection.

3.2 Delay differential equation and RNN

To compute the evolution (9) of \mathbf{x} , we consider an approximation of the Mori-Zwanzig memory term by a neural net ε with time convolution of \mathbf{x} as follows,

$$\int_0^t \mathbf{k}(t-s, \mathbf{x}(s)) \, ds \approx \varepsilon(\mathbf{x}(t), \mathbf{h}(t); \boldsymbol{\eta}) \quad \text{where} \quad \mathbf{h}(t) = \int_0^t \mathbf{K}(t-s; \mathbf{w})\mathbf{x}(s) \, ds. \quad (10)$$

In (10), $\mathbf{K}(\cdot; \mathbf{w})$ is a convolutional operator with parameter \mathbf{w} , and $\varepsilon(\mathbf{x}, \mathbf{h}; \boldsymbol{\eta})$ is a deep neural net with (\mathbf{x}, \mathbf{h}) as input and $\boldsymbol{\eta}$ as parameter. Both \mathbf{w} and $\boldsymbol{\eta}$ are to be trained by the cascade data \mathcal{D} . Hence, (9) reduces to the *delay differential equation* which involves a time integral $\mathbf{h}(t)$ of past \mathbf{x} :

$$\mathbf{x}' = \tilde{\mathbf{f}}(\mathbf{x}, \mathbf{h}; \boldsymbol{\theta}) := \mathbf{f}(\mathbf{x}; \mathbf{A}) + \varepsilon(\mathbf{x}, \mathbf{h}; \boldsymbol{\eta}). \quad (11)$$

The initial condition of (11) with source set \mathcal{S} is given by

$$\mathbf{x}(0) = \chi_{\mathcal{S}}, \quad \mathbf{h}(0) = \mathbf{0}, \quad \text{and} \quad \mathbf{x}(t) = \mathbf{h}(t) = \mathbf{0}, \quad \forall t < 0. \quad (12)$$

We call the system (11) with initial (12) the *neural mean-field* (NMF) dynamics.

The delay differential equation (11) is equivalent to a coupled system of (\mathbf{x}, \mathbf{h}) . In addition, we show that the discretization of this system reduces to a recurrent neural network if $\mathbf{K}(t; \mathbf{w})$ is a (linear combination of) matrix convolutions.

Theorem 3. *The delay differential equation (11) is equivalent to the following coupled system:*

$$\mathbf{x}' = \tilde{\mathbf{f}}(\mathbf{x}, \mathbf{h}; \mathbf{A}, \boldsymbol{\eta}) = \mathbf{f}(\mathbf{x}; \mathbf{A}) + \boldsymbol{\varepsilon}(\mathbf{x}, \mathbf{h}; \boldsymbol{\eta}) \quad (13a)$$

$$\mathbf{h}' = \int_0^t \mathbf{K}(t-s; \mathbf{w}) \tilde{\mathbf{f}}(\mathbf{x}(s), \mathbf{h}(s); \mathbf{A}, \boldsymbol{\eta}) ds \quad (13b)$$

with initial condition (12). In particular, if $\mathbf{K}(t; \mathbf{w}) = \sum_{l=1}^L \mathbf{B}_l e^{-\mathbf{C}_l t}$ for some $L \in \mathbb{N}$ with $\mathbf{w} = \{(\mathbf{B}_l, \mathbf{C}_l)_l : \mathbf{B}_l \mathbf{C}_l = \mathbf{C}_l \mathbf{B}_l, \forall l \in [L]\}$, then (13) can be solved by a non-delay system with $\mathbf{h}' = \sum_{l=1}^L (\mathbf{B}_l \mathbf{x} - \mathbf{C}_l \mathbf{h})$. The discretization of such system (with step size normalized to 1) reduces to an RNN of \mathbf{h}_t for $t = 0, 1, \dots, T-1$:

$$\mathbf{x}_{t+1} = \mathbf{x}_t + \mathbf{f}(\mathbf{x}_t; \mathbf{A}) + \boldsymbol{\varepsilon}(\mathbf{x}_t, \mathbf{h}_t; \boldsymbol{\eta}) \quad (14a)$$

$$\mathbf{h}_{t+1} = \mathbf{h}_t + \sum_{l=1}^L (\mathbf{B}_l \mathbf{x}_{t+1} - \mathbf{C}_l \mathbf{h}_t) \quad (14b)$$

with input $\mathbf{x}_0 = \chi_{\mathcal{S}}$ and $\mathbf{h}_0 = \mathbf{0}$.

The matrices \mathbf{B}_l and \mathbf{C}_l in (14b) correspond to the weights on \mathbf{x}_{t+1} and \mathbf{h}_t of the *linear* part in the first layer of the RNN, the approximate memory term $\boldsymbol{\varepsilon}$ constitutes the remaining *nonlinear* part.

We here consider a more general convolution kernel $\mathbf{K}(\cdot; \mathbf{w})$ than the exponential kernel. Note that, in practice, the convolution weight \mathbf{K} on past state \mathbf{x} in (10) rapidly decays, and hence the memory kernel \mathbf{K} can be well approximated with a truncated length $\tau \in \mathbb{N}$. Hence, we substitute (14b) by

$$\mathbf{h}_t = \mathbf{K}^{\mathbf{w}} \mathbf{m}_t \quad \text{where} \quad \mathbf{K}^{\mathbf{w}} = [\mathbf{K}_0^{\mathbf{w}}, \dots, \mathbf{K}_{\tau}^{\mathbf{w}}] \quad \text{and} \quad \mathbf{m}_t = [\mathbf{x}_t; \dots; \mathbf{x}_{t-\tau}]. \quad (15)$$

Then we formulate the evolution of the augmented state \mathbf{m}_t defined in (15) and follow (14a) to obtain a single evolution of \mathbf{m}_t for $t = 0, \dots, T-1$:

$$\mathbf{m}_{t+1} = \mathbf{g}(\mathbf{m}_t; \boldsymbol{\theta}), \quad \text{where} \quad \mathbf{g}(\mathbf{m}; \boldsymbol{\theta}) := [\mathbf{J}_0 \mathbf{m} + \tilde{\mathbf{f}}(\mathbf{J}_0 \mathbf{m}, \mathbf{K}^{\mathbf{w}} \mathbf{m}; \boldsymbol{\theta}); \mathbf{J}_0 \mathbf{m}; \dots; \mathbf{J}_{\tau-1} \mathbf{m}] \quad (16)$$

and $\mathbf{J}_s := [\dots, \mathbf{I}, \dots] \in \mathbb{R}^{n \times (\tau+1)n}$ has identity \mathbf{I} as the $(s+1)$ th block and $\mathbf{0}$ elsewhere. If (14b) is considered, a simpler augmented state $\mathbf{m}_t = [\mathbf{x}_t; \mathbf{h}_t]$ can be formed similarly; we omit the details here. We will use the dynamics (16) of the augmented state \mathbf{m}_t in the training below.

3.3 An optimal control formulation of parameter learning

Now we consider the training of the network parameters $\boldsymbol{\theta} = (\mathbf{A}, \boldsymbol{\eta}, \mathbf{w})$. Given a sample cascade $\hat{\mathbf{x}} = (\mathcal{S}, \boldsymbol{\tau})$ from \mathcal{D} , we can observe its value in $\{0, 1\}^n$ at each of the time points $t = 1, \dots, T$. The log-likelihood of $\hat{\mathbf{x}}$ given $\mathbf{x} = \mathbf{x}(\boldsymbol{\theta})$ is given by the loss function $\ell(\mathbf{x}, \hat{\mathbf{x}})$ defined by

$$\ell(\mathbf{x}, \hat{\mathbf{x}}) = \sum_{t=1}^T \hat{\mathbf{x}}_t \cdot \log \mathbf{x}_t + (\mathbf{1} - \hat{\mathbf{x}}_t) \cdot \log(\mathbf{1} - \mathbf{x}_t), \quad (17)$$

where the logarithm is taken componentwisely. We can further add regularization $r(\boldsymbol{\theta})$ to (17), such as l_2 -norm and/or other constraints on $\boldsymbol{\theta}$. In particular, if \mathcal{E} is known, we can require \mathbf{A} to be supported on \mathcal{E} . Otherwise, we can impose bounds on $\|\mathbf{A}\|_1$ or $\|\mathbf{A}\|_0$ (the l_1 or l_0 norm of the vectorized \mathbf{A}) if \mathcal{E} is expected to be sparse. In general, \mathbf{A} can be interpreted as the convolution to be learned from a graph convolution network (GCN) [30, 61]. The support and magnitude of \mathbf{A} implies the network structure and strength of interaction between pairs of nodes, respectively. We provide more details in Section 4.

Optimal parameter θ can be obtained by minimizing the loss function in (17). This procedure can also be cast as an optimal control problem to find θ that steers \mathbf{m}_t to fit data \mathcal{D} through (16):

$$\min_{\theta} \quad \mathcal{J}(\theta) := (1/K) \cdot \sum_{k=1}^K \ell(\mathbf{x}^{(k)}, \hat{\mathbf{x}}^{(k)}) + r(\theta) \quad (18a)$$

$$\text{s.t.} \quad \mathbf{m}_{t+1}^{(k)} = \mathbf{g}(\mathbf{m}_t^{(k)}; \theta), \quad \mathbf{m}_0^{(k)} = [\chi_{S_k}, \mathbf{0}, \dots, \mathbf{0}], \quad t \in [T] - 1, k \in [K], \quad (18b)$$

where $\mathbf{x}_t = \mathbf{J}_0 \mathbf{m}_t$ for all t . Define the *Hamiltonian*

$$H(\mathbf{m}, \mathbf{p}; \theta) = \mathbf{p} \cdot \mathbf{g}(\mathbf{m}; \theta) - \frac{1}{T} r(\theta), \quad (19)$$

then we can show that the optimal solution θ^* is a time invariant control satisfying a modified Pontryagin's Maximum Principle [3, 37] as follows.

Theorem 4. *Let \mathbf{x}^* be the optimally controlled state process by θ^* , then there exists a co-state (adjoint) \mathbf{p}^* which satisfies the backward differential equation*

$$\mathbf{m}_{t+1}^* = \mathbf{g}(\mathbf{m}_t^*; \theta^*), \quad \mathbf{m}_0^* = [\chi_{S_k}; \mathbf{0}; \dots; \mathbf{0}], \quad t = 0, \dots, T-1, \quad (20a)$$

$$\mathbf{p}_t^* = \mathbf{p}_{t+1}^* \cdot \nabla_{\mathbf{m}} \mathbf{g}(\mathbf{m}_t^*; \theta^*), \quad \mathbf{p}_T^* = -\nabla_{\mathbf{m}_T} \ell, \quad t = T-1, \dots, 0. \quad (20b)$$

Moreover, the optimal θ^* maximizes the total Hamiltonian: for any θ , there is

$$\sum_{t=0}^{T-1} H(\mathbf{m}_t^*, \mathbf{p}_{t+1}^*; \theta^*) \geq \sum_{t=0}^{T-1} H(\mathbf{m}_t^*, \mathbf{p}_{t+1}^*; \theta). \quad (21)$$

In addition, for any given θ , there is $\nabla_{\theta} \mathcal{J}(\theta) = -\sum_{t=0}^{T-1} \partial_{\theta} H(\mathbf{m}_t^{\theta}, \mathbf{p}_{t+1}^{\theta}; \theta)$, where $\{\mathbf{m}_t^{\theta}, \mathbf{p}_t^{\theta} : 0 \leq t \leq T\}$ are obtained by the forward and backward passes using (20a)-(20b) with this θ .

Proof is given in Appendix A. We introduced *total Hamiltonian* $\sum_{t=0}^{T-1} H(\mathbf{m}_t, \mathbf{p}_{t+1}; \theta)$ in Theorem 4 since the NMF dynamics (14) (or (16)) suggest a *time invariant* control θ independent of t , which corresponds to θ shared by all layers in an RNN. This is particularly important for time series analysis, where we perform regression on data observed within limited time window, but often want to use the learned parameters to predict events in distant future. Theorem 4 also implies that performing gradient descent to minimize \mathcal{J} in (18a) (often with back-propagation, as we used in NMF training) can be considered as attempting to maximize the total Hamiltonian in light of (21).

4 Numerical Experiments

Infection probability and influence function estimation We first test NMF on synthetic networks that mimic the structure of real-world diffusion network. Two types of Kronecker graph model [32] are used: hierarchical (Hier) network [10] and core-periphery (Core) network [33] with parameter matrices $[0.9, 0.1; 0.1, 0.9]$ and $[0.9, 0.5; 0.5, 0.3]$, respectively. For each type of network model, we generate 5 networks consisting of 128 nodes and 512 edges. We simulate the diffusion where the infection time are modeled by exponential distribution (Exp) and Rayleigh distribution (Ray). For each distribution, we draw α_{ji} from Unif[1,10] to simulate the varying interactions between nodes. Training data has 10 cascades for each of 1,000 source sets (size between 1 and 10), total of $K=10,000$ cascades. All networks and cascades are generated by SNAP [34].

We compare NMF to two baseline methods: InfluenLearner [14] which is a state-of-the-art method that learns the coverage function of each node for any fixed time, and a conditional LSTM (LSTM for short) [24], which are among the few existing methods capable of learning infection probabilities of individual nodes directly from cascade data as ours. For InfluenLearner, we set 128 as the features amount for optimal accuracy as suggested in [14]. For LSTM, we use one LSTM block for each t . To evaluate accuracy, we compute the Mean Absolute Error (MAE) of node infection probability $\|\mathbf{x}_t - \mathbf{x}_t^*\|_1/n$ and influence $|\mathbf{1} \cdot (\mathbf{x}_t - \mathbf{x}_t^*)|$, averaged over the 100 source sets for each time t , where \mathbf{x}^* is obtained by averaging 10,000 MC simulations for each source set, and \mathbf{x} is the result obtained by the compared methods. The results are shown in Figure 1, which shows the mean (center line) and standard deviation (shade) of the three methods. NMF generally has lowest MAE, except at some early stages where InfluenLearner is better. Note that InfluenLearner benefits

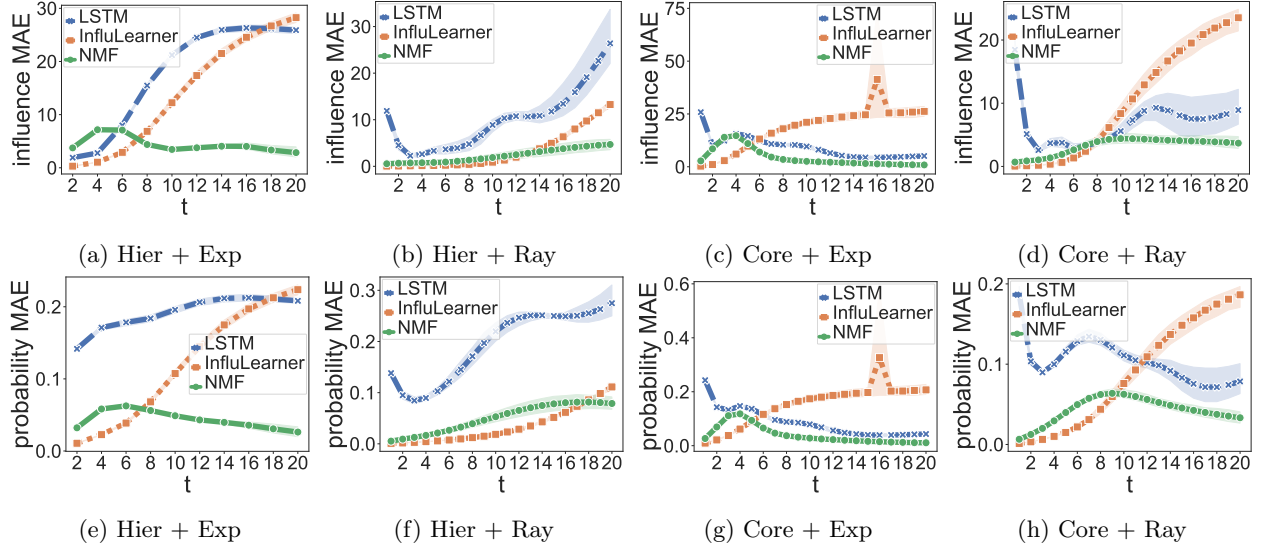


Figure 1: MAE of influence (top row) and node infection probability (bottom row) by LSTM, InfluenLearner, and NMF on different combinations of Hierarchical (Hier) and Core-periphery (Core) networks, and exponential (Exp) and Rayleigh (Ray) diffusion models. Mean (centerline) and standard deviation (shade) over 100 tests are shown.

from the knowledge of the original source node for each infection in the cascade (provided in our training data), which is often unavailable in practice and not needed in our method.

We also tested NMF on a real dataset [63] from Sina Weibo social platform consisting of more than 1.78 million users and 308 million following relationships among them. From past 1,000 tweets of each user we select the most popular tweet to generate diffusion cascades. Following the setting in [14], we recreate cascades by only keeping nodes of the top 1,000 frequency in the pooled node set over all cascades. For testing, we uniformly generate 100 source sets of size 10 and use $t = 1, 2, \dots, 10$ as the time steps for observation. Finally, we test 100 source sets and compare our model NMF with the InfluenLearner and LSTM. The MAE of all methods are shown in Figure 2a. We can see that the performance of NMF is more robust than LSTM, and similar as InfluenLearner. However, unlike InfluenLearner that requires re-training for *every* t and is computationally expensive, NMF learns the evolution at all t in a single sweep of training and is tens of time faster.

We also test robustness of NMF for varying network density $|\mathcal{E}|/n$. The MAE of influence and infection probability by NMF on a hierarchical network with $n = 128$ are shown in Figure 2c and 2b, respectively. NMF remains accurate for denser networks, which can be notoriously difficult for other methods such as InfluenLearner.

Network Structure Inference The interpretable parameterization of NMF allows us to explicitly learn the weight matrix \mathbf{A} . In this test, we examine the quality of the learned \mathbf{A} . We set the recovered adjacency matrix \mathcal{E} to the binary indicator matrix $\mathbf{A}^\top \geq \epsilon$, i.e., $(\mathcal{E})_{i,j} = 1$ if $(\mathbf{A})_{ji} \geq 0.01$. To evaluate the quality of \mathcal{E} and \mathbf{A} , we use four metrics: precision (Prc), recall (Rcl), accuracy (Acc), and correlation (Cor), defined as follows,

$$\text{Prc}(\mathcal{E}, \mathcal{E}^*) = \frac{|\mathcal{E} \cap \mathcal{E}^*|}{|\mathcal{E}|}, \quad \text{Rcl}(\mathcal{E}, \mathcal{E}^*) = \frac{|\mathcal{E} \cap \mathcal{E}^*|}{|\mathcal{E}^*|}, \quad \text{Acc}(\mathcal{E}, \mathcal{E}^*) = 1 - \frac{|\mathcal{E} \oplus \mathcal{E}^*|}{|\mathcal{E}| + |\mathcal{E}^*|}, \quad \text{Cor}(\mathbf{A}, \mathbf{A}^*) = \frac{\text{tr}(\mathbf{A}^\top \mathbf{A}^*)}{\|\mathbf{A}\|_F \|\mathbf{A}^*\|_F}.$$

where \mathcal{E}^* and \mathbf{A}^* are their true values, respectively. In Acc, the edge set \mathcal{E} is also interpreted as a matrix, and $|\mathcal{E}|$ counts the number of nonzeros in \mathcal{E} . In Cor, $\|\mathbf{A}\|_F^2 = \text{tr}(\mathbf{A}^\top \mathbf{A})$ is the Frobenius norm of the matrix \mathbf{A} . Prc is the ratio of edges in \mathcal{E}^* that are recovered in \mathcal{E} . Rcl is the ratio of correctly recovered edges in \mathcal{E} . Acc indicates the ratio of the number of common edges shared by \mathcal{E} and \mathcal{E}^* against the total number of edges in them. Cor measures similarity between \mathbf{A} and \mathbf{A}^* by taking their values into consideration. All

Table 1: Performance of structure inference using NETRATE and the proposed NMF on Random, Hierarchical, and Core-periphery networks with Rayleigh as diffusion distribution on edges. Quality of the learned edge set \mathcal{E} and distribution parameter \mathbf{A} are measured by precision (Prc), recall (Rcl), accuracy (Acc), and correlation (Cor). Higher value indicates better quality.

Network	Method	Prc	Rcl	Acc	Cor
Random	NETRATE	0.481	0.399	0.434	0.120
	NMF	0.858	0.954	0.903	0.412
Hierarchical	NETRATE	0.659	0.429	0.519	0.129
	NMF	0.826	0.978	0.893	0.488
Core-periphery	NETRATE	0.150	0.220	0.178	0.045
	NMF	0.709	0.865	0.779	0.338

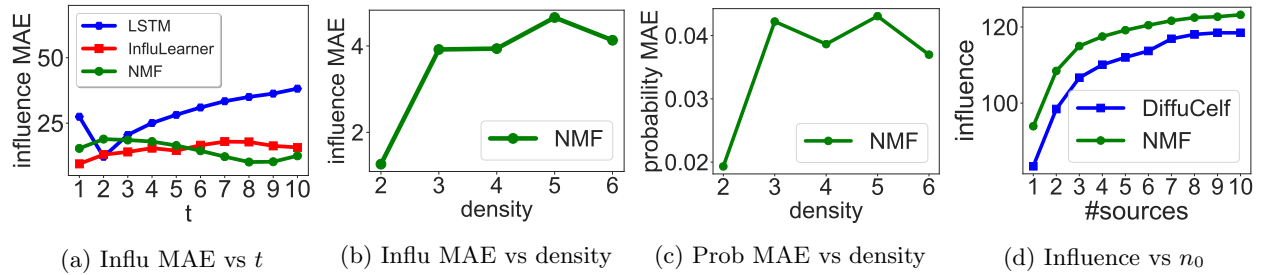


Figure 2: (a) MAE of influence estimated by LSTM, InfluenLearner on Weibo data; (b)–(c) MAE of influence and infection probability of NMF for different network densities; (d) Influence of source sets selected by DIFFUCELFF and NMF+Greedy for $n_0 = 1, \dots, 10$.

metrics are bounded between $[0, 1]$, and higher value indicates better result. For comparison, we also test NETRATE [20] to the cascade data and learn \mathbf{A} with Rayleigh distribution. Evaluation by four metrics are shown in Table 1, which indicates that NMF outperforms NETRATE in all metrics. Note that NMF learns \mathbf{A} along with infection probability in its training, whereas NETRATE can only learn the matrix \mathbf{A} .

Influence Maximization We use NMF as an influence estimation subroutine in a classical greedy algorithm [46] (NMF+Greedy), and compare with a state-of-the-art method DIFFCELFF [50] for influence maximization (IM). Like NMF+Greedy, DIFFCELFF also only requires infection time features, but not network structures as in most existing methods. We generate 1000 cascades with unique source (as required by DIFFCELFF but not ours) on a hierarchical network of 128 nodes and 512 edges, and use exponential distribution for the transmission function with \mathbf{A} generated from Unif[1,10]. Time window is $T = 20$. For each source set size $n_0 = 1, \dots, 10$, NMF+Greedy and DIFFCELFF are applied to identify the optimal source sets, whose influence are computed by averaging 10,000 MC simulated cascades. Figure 2d shows that the source sets obtained by NMF+Greedy generates greater influence than DIFFCELFF consistently for every source size n_0 .

5 Related Work

Inference and estimation for diffusion networks have attracted great attentions from both researchers and practitioners, especially with the flourish of social media [6, 7, 35, 36, 38, 52, 54, 56, 59, 65, 66, 68]. SEISMIC [65] is an implementation of Hawkes self-exciting point process to capture the cascading effect and predict its impact on self-exciting mechanism. Power-law function is use to fit the time decay effect in information diffusion

with prior information obtained from training data. DeepCas [36] utilized the structural and node identities features from the representation cascade graphs in an end-to-end manner to predict the future incremental influence (popularity). DeepHawkes [52] learns the interpretable factors of Hawkes process (influence of user, self-exciting mechanism of each retweet and the time decay effect) under deep learning framework with features only from information cascades. CoupledGNN [7] utilizes two coupled neural networks to iteratively capture the cascading effect in information diffusion to predict future popularity. MMVED [68] applies convolutional neural network (CNN) to extract features and recurrent neural network (RNN) to capture the temporal relationships on the user-generated contents networks (eg. Views, likes, comments, reposts). Deepinf [54] is an end-to-end framework for social influence estimation which incorporate both network structures and user specific features into convolutional neural and attention networks to learn users’s latent feature representation, and the extended DeepInf [35] enhance the performance of DeepInf by integrating teleport probability from the domain of page rank into the graph convolution network (GCN) model. Unlike these methods, NMF does not require early adopters or network structure to capture cascade effect. Moreover, NMF can estimate the infection probability of every node, not just the overall influence.

Similar to ours, [14] also learns to estimate influence functions from observed cascades. In [14], the authors propose a parameterization of the coverage function that can be learned for influence prediction. The Probably Approximately Correct (PAC) learnability of influence functions for Linear Threshold (LT), Independent Cascade (IC) and Voter models with partial or full observations is considered in [45], which provides theoretical evidence of the direct modeling capabilities from samples. In particular, the authors show that LT influence functions can be seen as multi-layer neural network classifiers, and proceed by bounding their Vapnik-Chervonenkis (VC) dimension. In the present work, we show that time discretization of the derived NMF reduces to a structured and interpretable RNN, where important diffusion parameters can be efficiently learned from cascade data directly.

6 Conclusion

We propose a novel framework using neural mean-field dynamics for inference and estimation on diffusion networks. Our new framework is derived from the Mori-Zwanzig formalism to obtain exact evolution of node infection probabilities. The memory term of the Mori-Zwanzig equation can be approximated by convolutions, which renders the system as a delay differential equation and its time discretization reduces to a structured and interpretable RNN. Empirical study shows that our approach is versatile and robust to different variations of diffusion network models, and significantly outperform existing approaches in accuracy and efficiency on both synthetic and real-world data.

References

- [1] M. Abadi, P. Barham, J. Chen, Z. Chen, A. Davis, J. Dean, M. Devin, S. Ghemawat, G. Irving, M. Isard, M. Kudlur, J. Levenberg, R. Monga, S. Moore, D. G. Murray, B. Steiner, P. Tucker, V. Vasudevan, P. Warden, M. Wicke, Y. Yu, and X. Zheng. Tensorflow: A system for large-scale machine learning, 2016.
- [2] B. Abrahao, F. Chierichetti, R. Kleinberg, and A. Panconesi. Trace complexity of network inference. In *Proceedings of the 19th ACM SIGKDD international conference on Knowledge discovery and data mining*, pages 491–499, 2013.
- [3] D. P. Bertsekas. *Dynamic programming and optimal control*, volume 1. Athena scientific Belmont, MA, 1995.
- [4] Á. Bodó, G. Y. Katona, and P. L. Simon. Sis epidemic propagation on hypergraphs. *Bulletin of mathematical biology*, 78(4):713–735, 2016.
- [5] M. Boguná and R. Pastor-Satorras. Epidemic spreading in correlated complex networks. *Physical Review E*, 66(4):047104, 2002.
- [6] Q. Cao, H. Shen, K. Cen, W. Ouyang, and X. Cheng. Deephawkes: Bridging the gap between prediction and understanding of information cascades. In *Proceedings of the 2017 ACM on Conference on Information and Knowledge Management*, pages 1149–1158, 2017.
- [7] Q. Cao, H. Shen, J. Gao, B. Wei, and X. Cheng. Popularity prediction on social platforms with coupled graph neural networks. In *Proceedings of the 13th International Conference on Web Search and Data Mining*, WSDM ’20, pages 70–78, New York, NY, USA, 2020. Association for Computing Machinery.
- [8] W. Chen, Y. Wang, and S. Yang. Efficient influence maximization in social networks. In *Proceedings of the 15th ACM SIGKDD International Conference on Knowledge Discovery and Data Mining*, KDD ’09, pages 199–208, New York, NY, USA, 2009. Association for Computing Machinery.
- [9] A. J. Chorin, O. H. Hald, and R. Kupferman. Optimal prediction and the mori–zwanzig representation of irreversible processes. *Proceedings of the National Academy of Sciences*, 97(7):2968–2973, 2000.
- [10] A. Clauset, C. Moore, and M. E. J. Newman. Hierarchical structure and the prediction of missing links in networks. *Nature*, 453(7191):98–101, May 2008.
- [11] E. Cohen, D. Delling, T. Pajor, and R. F. Werneck. Sketch-based influence maximization and computation: Scaling up with guarantees. In *Proceedings of the 23rd ACM International Conference on Conference on Information and Knowledge Management*, CIKM ’14, pages 629–638, New York, NY, USA, 2014. Association for Computing Machinery.
- [12] H. Daneshmand, M. Gomez-Rodriguez, L. Song, and B. Schölkopf. Estimating diffusion network structures: Recovery conditions, sample complexity & soft-thresholding algorithm. In *International Conference on Machine Learning*, pages 793–801, 2014.
- [13] M. Draief, A. Ganesh, and L. Massoulié. Thresholds for virus spread on networks. In *Proceedings of the 1st International Conference on Performance Evaluation Methodologies and Tools*, valuetools ’06, pages 51–es, New York, NY, USA, 2006. Association for Computing Machinery.
- [14] N. Du, Y. Liang, M.-F. Balcan, and L. Song. Influence function learning in information diffusion networks. In *Proceedings of the 31st International Conference on International Conference on Machine Learning - Volume 32*, ICML’14, pages II–2016–II–2024. JMLR.org, 2014.
- [15] N. Du, Y. Liang, M.-F. Balcan, and L. Song. Influence function learning in information diffusion networks. In *International Conference on Machine Learning*, pages 2016–2024, 2014.
- [16] N. Du, L. Song, M. Gomez-Rodriguez, and H. Zha. Scalable influence estimation in continuous-time diffusion networks. In *Advances in Neural Information Processing Systems*, pages 3147–3155, 2013.

- [17] N. Du, L. Song, M. Gomez-Rodriguez, and H. Zha. Scalable influence estimation in continuous-time diffusion networks. In *Proceedings of the 26th International Conference on Neural Information Processing Systems - Volume 2*, NIPS'13, pages 3147–3155, Red Hook, NY, USA, 2013. Curran Associates Inc.
- [18] Eun Jee Lee, S. Kamath, E. Abbe, and S. R. Kulkarni. Spectral bounds for independent cascade model with sensitive edges. In *2016 Annual Conference on Information Science and Systems (CISS)*, pages 649–653, 2016.
- [19] M. Farajtabar, X. Ye, S. Harati, L. Song, and H. Zha. Multistage campaigning in social networks. In *Advances in Neural Information Processing Systems*, pages 4718–4726, 2016.
- [20] M. Gomez-Rodriguez, D. Balduzzi, and B. Schölkopf. Uncovering the temporal dynamics of diffusion networks. *arXiv preprint arXiv:1105.0697*, 2011.
- [21] M. Gomez-Rodriguez, D. Balduzzi, and B. Schölkopf. Uncovering the temporal dynamics of diffusion networks. In *Proceedings of the 28th International Conference on International Conference on Machine Learning*, ICML'11, pages 561–568, Madison, WI, USA, 2011. Omnipress.
- [22] M. Gomez-Rodriguez, J. Leskovec, and A. Krause. Inferring networks of diffusion and influence. *CoRR*, abs/1006.0234, 2010.
- [23] M. Gomez-Rodriguez, J. Leskovec, and B. Schölkopf. Structure and dynamics of information pathways in online media. *CoRR*, abs/1212.1464, 2012.
- [24] S. Hochreiter and J. Schmidhuber. Long short-term memory. *Neural computation*, 9:1735–80, 12 1997.
- [25] K. Jung, W. Heo, and W. Chen. Irie: Scalable and robust influence maximization in social networks. In *Proceedings of the 2012 IEEE 12th International Conference on Data Mining*, ICDM '12, pages 918–923, USA, 2012. IEEE Computer Society.
- [26] D. Kempe, J. Kleinberg, and É. Tardos. Maximizing the spread of influence through a social network. In *Proceedings of the ninth ACM SIGKDD international conference on Knowledge discovery and data mining*, pages 137–146. ACM, 2003.
- [27] D. Kempe, J. Kleinberg, and E. Tardos. Maximizing the spread of influence through a social network. In *Proceedings of the Ninth ACM SIGKDD International Conference on Knowledge Discovery and Data Mining*, pages 137–146. Association for Computing Machinery, 2003.
- [28] D. Kempe, J. Kleinberg, and É. Tardos. Influential nodes in a diffusion model for social networks. In *Automata, languages and programming*, pages 1127–1138. Springer, 2005.
- [29] M. Kimura and K. Saito. Tractable models for information diffusion in social networks. In *European Conference on Principles of Data Mining and Knowledge Discovery*, pages 259–271, 09 2006.
- [30] T. N. Kipf and M. Welling. Semi-supervised classification with graph convolutional networks. *arXiv preprint arXiv:1609.02907*, 2016.
- [31] R. Lemonnier, K. Scaman, and N. Vayatis. Tight bounds for influence in diffusion networks and application to bond percolation and epidemiology, 2014.
- [32] J. Leskovec, D. Chakrabarti, J. Kleinberg, C. Faloutsos, and Z. Ghahramani. Kronecker graphs: An approach to modeling networks. *The Journal of Machine Learning Research*, 11:985–1042, 2010.
- [33] J. Leskovec, K. J. Lang, A. Dasgupta, and M. W. Mahoney. Statistical properties of community structure in large social and information networks. In *Proceedings of the 17th International Conference on World Wide Web*, WWW '08, pages 695–704, New York, NY, USA, 2008. Association for Computing Machinery.
- [34] J. Leskovec and R. Sosič. Snap: A general-purpose network analysis and graph-mining library. *ACM Transactions on Intelligent Systems and Technology (TIST)*, 8(1):1, 2016.

- [35] C. K. Leung, A. Cuzzocrea, J. J. Mai, D. Deng, and F. Jiang. Personalized deepinf: Enhanced social influence prediction with deep learning and transfer learning. In *2019 IEEE International Conference on Big Data (Big Data)*, pages 2871–2880, 2019.
- [36] C. Li, J. Ma, X. Guo, and Q. Mei. Deepcas: An end-to-end predictor of information cascades. In *Proceedings of the 26th international conference on World Wide Web*, pages 577–586, 2017.
- [37] Q. Li, L. Chen, C. Tai, and E. Weinan. Maximum principle based algorithms for deep learning. *The Journal of Machine Learning Research*, 18(1):5998–6026, 2017.
- [38] D. Liao, J. Xu, G. Li, W. Huang, W. Liu, and J. Li. Popularity prediction on online articles with deep fusion of temporal process and content features. In *Proceedings of the AAAI Conference on Artificial Intelligence*, volume 33, pages 200–207, 2019.
- [39] Q. Liu, B. Xiang, E. Chen, H. Xiong, F. Tang, and J. X. Yu. Influence maximization over large-scale social networks: A bounded linear approach. In *Proceedings of the 23rd ACM International Conference on Conference on Information and Knowledge Management, CIKM '14*, pages 171–180, New York, NY, USA, 2014. Association for Computing Machinery.
- [40] A. Lokhov. Reconstructing parameters of spreading models from partial observations. In D. D. Lee, M. Sugiyama, U. V. Luxburg, I. Guyon, and R. Garnett, editors, *Advances in Neural Information Processing Systems 29*, pages 3467–3475. Curran Associates, Inc., 2016.
- [41] A. Y. Lokhov and D. Saad. Scalable influence estimation without sampling. *arXiv preprint arXiv:1912.12749*, 2019.
- [42] B. Lucier, J. Oren, and Y. Singer. Influence at scale: Distributed computation of complex contagion in networks. In *Proceedings of the 21th ACM SIGKDD International Conference on Knowledge Discovery and Data Mining, KDD '15*, pages 735–744, New York, NY, USA, 2015. Association for Computing Machinery.
- [43] J. C. Miller and I. Z. Kiss. Epidemic spread in networks: Existing methods and current challenges. *Mathematical modelling of natural phenomena*, 9(2):4, 2014.
- [44] S. Myers and J. Leskovec. On the convexity of latent social network inference. In *Advances in neural information processing systems*, pages 1741–1749, 2010.
- [45] H. Narasimhan, D. C. Parkes, and Y. Singer. Learnability of influence in networks. In *Advances in Neural Information Processing Systems*, pages 3186–3194, 2015.
- [46] G. L. Nemhauser, L. A. Wolsey, and M. L. Fisher. An analysis of approximations for maximizing submodular set functions—i. *Mathematical programming*, 14(1):265–294, 1978.
- [47] P. Netrapalli and S. Sanghavi. Learning the graph of epidemic cascades. *ACM SIGMETRICS Performance Evaluation Review*, 40(1):211–222, 2012.
- [48] M. Newman. *Networks: an introduction*. Oxford University Press, 2010.
- [49] H. T. Nguyen, T. P. Nguyen, T. N. Vu, and T. N. Dinh. Outward influence and cascade size estimation in billion-scale networks. *Proc. ACM Meas. Anal. Comput. Syst.*, 1(1), June 2017.
- [50] G. Panagopoulos, F. D. Malliaros, and M. Vazirgiannis. Diffugreedy: an influence maximization algorithm based on diffusion cascades. In *International Conference on Complex Networks and their Applications*, pages 392–404. Springer, 2018.
- [51] R. Pastor-Satorras, C. Castellano, P. Van Mieghem, and A. Vespignani. Epidemic processes in complex networks. *Reviews of modern physics*, 87(3):925, 2015.
- [52] B. Perozzi, R. Al-Rfou, and S. Skiena. Deepwalk: Online learning of social representations. In *Proceedings of the 20th ACM SIGKDD international conference on Knowledge discovery and data mining*, pages 701–710, 2014.

- [53] J. Pouget-Abadie and T. Horel. Inferring graphs from cascades: A sparse recovery framework. *arXiv preprint arXiv:1505.05663*, 2015.
- [54] J. Qiu, J. Tang, H. Ma, Y. Dong, K. Wang, and J. Tang. Deepinf: Social influence prediction with deep learning. In *Proceedings of the 24th ACM SIGKDD International Conference on Knowledge Discovery & Data Mining*, pages 2110–2119, 2018.
- [55] F. D. Sahneh and C. Scoglio. Epidemic spread in human networks. In *Decision and Control and European Control Conference (CDC-ECC), 2011 50th IEEE Conference on*, pages 3008–3013. IEEE, 2011.
- [56] J. Shao, H. Shen, Q. Cao, and X. Cheng. Temporal convolutional networks for popularity prediction of messages on social medias. In *China Conference on Information Retrieval*, pages 135–147. Springer, 2019.
- [57] P. Van Mieghem, J. Omic, and R. Kooij. Virus spread in networks. *Networking, IEEE/ACM Transactions on*, 17(1):1–14, 2009.
- [58] M. Vergeer, L. Hermans, and S. Sams. Online social networks and micro-blogging in political campaigning the exploration of a new campaign tool and a new campaign style. *Party Politics*, 19(3):477–501, 2013.
- [59] X. Wang, Z. Guo, X. Wang, S. Liu, W. Jing, and Y. Liu. Nnmlinf: social influence prediction with neural network multi-label classification. In *Proceedings of the ACM Turing Celebration Conference-China*, pages 1–5, 2019.
- [60] J. Wortman. Viral marketing and the diffusion of trends on social networks. *Tech Report*, 2008.
- [61] Z. Wu, S. Pan, F. Chen, G. Long, C. Zhang, and P. S. Yu. A comprehensive survey on graph neural networks. *IEEE Transactions on Neural Networks and Learning Systems*, pages 1–21, 2020.
- [62] Y. Yang, E. Chen, Q. Liu, B. Xiang, T. Xu, and S. A. Shad. On approximation of real-world influence spread. In P. A. Flach, T. De Bie, and N. Cristianini, editors, *Machine Learning and Knowledge Discovery in Databases*, pages 548–564, Berlin, Heidelberg, 2012. Springer Berlin Heidelberg.
- [63] J. Zhang, B. Liu, J. Tang, T. Chen, and J. Li. Social influence locality for modeling retweeting behaviors. In *Proceedings of the Twenty-Third International Joint Conference on Artificial Intelligence, IJCAI ’13*, pages 2761–2767. AAAI Press, 2013.
- [64] M. Zhang, C. Dai, C. Ding, and E. Chen. Probabilistic solutions of influence propagation on social networks. In *Proceedings of the 22nd ACM International Conference on Information and Knowledge Management, CIKM ’13*, pages 429–438, New York, NY, USA, 2013. Association for Computing Machinery.
- [65] Q. Zhao, M. A. Erdogdu, H. Y. He, A. Rajaraman, and J. Leskovec. Seismic: A self-exciting point process model for predicting tweet popularity. In *Proceedings of the 21th ACM SIGKDD International Conference on Knowledge Discovery and Data Mining*, pages 1513–1522, 2015.
- [66] C. Zheng, Q. Zhang, G. Long, C. Zhang, S. D. Young, and W. Wang. Measuring time-sensitive and topic-specific influence in social networks with lstm and self-attention. *IEEE Access*, 8:82481–82492, 2020.
- [67] C. Zhou, P. Zhang, W. Zang, and L. Guo. On the upper bounds of spread for greedy algorithms in social network influence maximization. *IEEE Transactions on Knowledge and Data Engineering*, 27(10):2770–2783, 2015.
- [68] Y. Zhu, J. Xie, and Z. Chen. Predicting the popularity of micro-videos with multimodal variational encoder-decoder framework, 2020.

A Proofs

A.1 Proof of Theorem 1

Proof of Theorem 1. Let $\mathbb{E}[\mathrm{d}X_i(t)|\mathcal{H}(t)] = \lambda_i^*(t) \mathrm{d}t$. In the standard diffusion model, the conditional intensity $\lambda_i^*(t)$ of a healthy node i ($X_i(t) = 0$) is determined by the total infection rate of its infected neighbors j ($X_j(t) = 1$), i.e.,

$$\lambda_i^*(t) = \sum_j \alpha_{ji} X_j(t) (1 - X_i(t)). \quad (22)$$

By taking expectation $\mathbb{E}_{\mathcal{H}(t)}[\cdot]$ on both sides of (22), we obtain

$$\begin{aligned} \lambda_i(t) &:= \mathbb{E}_{\mathcal{H}(t)}[\lambda_i^*(t)] = \mathbb{E}_{\mathcal{H}(t)} \left[\alpha_{ji} X_j(t) (1 - X_i(t)) | \mathcal{H}(t) \right] \\ &= \sum_j \alpha_{ji} (x_j - x_{ij}) = \sum_j \alpha_{ji} (x_j - y_{ij} - e_{ij}). \end{aligned} \quad (23)$$

On the other hand, there is

$$\lambda_i(t) \mathrm{d}t = \mathbb{E}_{\mathcal{H}(t)}[\lambda_i^*(t)] \mathrm{d}t = \mathbb{E}_{\mathcal{H}(t)}[\mathrm{d}X_i(t)|\mathcal{H}(t)] = \mathrm{d}\mathbb{E}_{\mathcal{H}(t)}[X_i(t)|\mathcal{H}(t)] = \mathrm{d}x_i. \quad (24)$$

Combining (23) and (24) yields

$$x'_i = \frac{\mathrm{d}x_i(t)}{\mathrm{d}t} = \sum_j \alpha_{ji} (x_j - y_{ij} - e_{ij}) = (\mathbf{A}\mathbf{x})_i - (\mathrm{diag}(\mathbf{x})\mathbf{A}\mathbf{x})_i - \sum_j \alpha_{ji} e_{ij}$$

for every $i \in [n]$, which verifies the \mathbf{x} part of (6). Similarly, we can obtain

$$x'_I = \sum_{i \in I} \sum_{j \notin I} \alpha_{ji} (x_I - x_{I \cup \{j\}}) = \sum_{i \in I} \sum_{j \notin I} \alpha_{ji} (y_I + e_I - y_{I \cup \{j\}} - e_{I \cup \{j\}}) \quad (25)$$

On the other hand, by taking derivative on both sides of $x_I(t) = y_I(t) + e_I(t)$, we obtain

$$x'_I = \sum_{i \in I} y_{I \setminus \{i\}} x'_i + e'_I = \sum_{i \in I} y_{I \setminus \{i\}} \sum_{j \neq i} \alpha_{ji} (x_j - x_i x_j - e_{ij}) + e'_I. \quad (26)$$

Combining (25) and (26) yields the \mathbf{e} part of (6).

It is clear that $\mathbf{x}_0 = \chi_{\mathcal{S}}$. For every I , at time $t = 0$, there is $x_I(0) = \prod_{i \in I} X_i(0) = 1$ if $I \subset \mathcal{S}$ and 0 otherwise; and the same for $y_I(0)$. Hence $e_I(0) = x_I(0) - y_I(0) = 0$ for all I . Hence $\mathbf{z}_0 = [\mathbf{x}_0; \mathbf{e}_0] = [\chi_{\mathcal{S}}; \mathbf{0}]$, which verifies the initial condition of (6). \square

A.2 Proof of Theorem 2

Proof of Theorem 2. Consider the system (6) over a finite time horizon $[0, T]$, which evolves on a smooth manifold $\Gamma \subset \mathbb{R}^N$. For any real-valued phase (observable) space function $g : \Gamma \rightarrow \mathbb{R}$, the nonlinear system (6) is equivalent to the linear partial differential equation, known as the Liouville equation:

$$\begin{cases} \partial_t u(t, \mathbf{z}) = \mathcal{L}[u](t, \mathbf{z}) \\ u(0, \mathbf{z}) = g(\mathbf{z}) \end{cases} \quad (27)$$

where the Liouville operator $\mathcal{L}[u] := \bar{\mathbf{f}}(\mathbf{z}) \cdot \nabla_{\mathbf{z}} u$. The equivalency is in the sense that the solution of (27) satisfies $u(t, \mathbf{z}_0) = g(\mathbf{z}(t; \mathbf{z}_0))$, where $\mathbf{z}(t; \mathbf{z}_0)$ is the solution to (6) with initial value \mathbf{z}_0 .

Denote $e^{t\mathcal{L}}$ the Koopman operator associated with \mathcal{L} such that $e^{t\mathcal{L}}g(\mathbf{z}_0) = g(\mathbf{z}(t))$ where $\mathbf{z}(t)$ is the solution of (6). Then $e^{t\mathcal{L}}$ satisfies the semi-group property, i.e.,

$$e^{t\mathcal{L}}g(\mathbf{z}) = g(e^{t\mathcal{L}}\mathbf{z}) \quad (28)$$

for all g . On the right hand side of (28), \mathbf{z} can be interpreted as $\mathbf{z} = \boldsymbol{\iota}(\mathbf{z}) = [\iota_1(\mathbf{z}), \dots, \iota_N(\mathbf{z})]$ where $\iota_j(\mathbf{z}) = z_j$ for all j .

Now consider the projection operator \mathcal{P} as the truncation such that $\mathcal{P}g(\mathbf{z}) = \mathcal{P}g(\mathbf{x}, \mathbf{e}) = g(\mathbf{x}, 0)$ for any $\mathbf{z} = (\mathbf{x}, \mathbf{e})$, and its orthogonal complement as $\mathcal{Q} = I - \mathcal{P}$ where I is the identity operator. Note that $\mathbf{z}'(t) = \frac{d\mathbf{z}(t)}{dt} = \frac{\partial}{\partial t} e^{t\mathcal{L}} \mathbf{z}_0$, and $\bar{\mathbf{f}}(\mathbf{z}(t)) = e^{t\mathcal{L}} \mathbf{f}(\mathbf{z}_0) = e^{t\mathcal{L}} \mathcal{L} \mathbf{z}_0$ since $\mathcal{L}\iota_j(\mathbf{z}) = \mathbf{f}_j(\mathbf{z})$ for all \mathbf{z} and j . Therefore (6) implies that

$$\frac{\partial}{\partial t} e^{t\mathcal{L}} \mathbf{z}_0 = e^{t\mathcal{L}} \mathcal{L} \mathbf{z}_0 = e^{t\mathcal{L}} \mathcal{P} \mathcal{L} \mathbf{z}_0 + e^{t\mathcal{L}} \mathcal{Q} \mathcal{L} \mathbf{z}_0. \quad (29)$$

Note that the first term on the right hand side of (29) is

$$e^{t\mathcal{L}} \mathcal{P} \mathcal{L} \mathbf{z}_0 = \mathcal{P} \mathcal{L} e^{t\mathcal{L}} \mathbf{z}_0 = \mathcal{P} \mathcal{L} \mathbf{z}(t). \quad (30)$$

For the second term in (29), we recall that the well-known Dyson's identity for the Koopman operator \mathcal{L} is given by

$$e^{t\mathcal{L}} = e^{t\mathcal{Q}\mathcal{L}} + \int_0^t e^{s\mathcal{L}} \mathcal{P} \mathcal{L} e^{(t-s)\mathcal{Q}\mathcal{L}} ds. \quad (31)$$

Applying (31) to $\mathcal{Q}\mathcal{L}\mathbf{z}_0$ yields

$$\begin{aligned} e^{t\mathcal{L}} \mathcal{Q}\mathcal{L}\mathbf{z}_0 &= e^{t\mathcal{Q}\mathcal{L}} \mathcal{Q}\mathcal{L}\mathbf{z}_0 + \int_0^t e^{s\mathcal{L}} \mathcal{P} \mathcal{L} e^{(t-s)\mathcal{Q}\mathcal{L}} \mathcal{Q}\mathcal{L}\mathbf{z}_0 ds \\ &= e^{t\mathcal{Q}\mathcal{L}} \mathcal{Q}\mathcal{L}\mathbf{z}_0 + \int_0^t \mathcal{P} \mathcal{L} e^{(t-s)\mathcal{Q}\mathcal{L}} \mathcal{Q}\mathcal{L} e^{s\mathcal{L}} \mathbf{z}_0 ds \\ &= e^{t\mathcal{Q}\mathcal{L}} \mathcal{Q}\mathcal{L}\mathbf{z}_0 + \int_0^t \mathcal{P} \mathcal{L} e^{(t-s)\mathcal{Q}\mathcal{L}} \mathcal{Q}\mathcal{L}\mathbf{z}(s) ds \end{aligned} \quad (32)$$

Substituting (30) and (32) into (29), we obtain

$$\frac{\partial}{\partial t} e^{t\mathcal{L}} \mathbf{z}_0 = \mathcal{P} \mathcal{L} \mathbf{z}(t) + e^{t\mathcal{Q}\mathcal{L}} \mathcal{Q}\mathcal{L}\mathbf{z}_0 + \int_0^t \mathcal{P} \mathcal{L} e^{(t-s)\mathcal{Q}\mathcal{L}} \mathcal{Q}\mathcal{L}\mathbf{z}(s) ds. \quad (33)$$

where we used the fact that $e^{t\mathcal{L}} \mathcal{P} \mathcal{L} \mathbf{z}_0 = \mathcal{P} \mathcal{L} e^{t\mathcal{L}} \mathbf{z}_0 = \mathcal{P} \mathcal{L} \mathbf{z}(t)$. Denote $\phi(t, \mathbf{z}) := e^{t\mathcal{L}} \mathcal{Q}\mathcal{L}\mathbf{z}$, then we simplify (33) into

$$\frac{\partial}{\partial t} e^{t\mathcal{L}} \mathbf{z}_0 = \mathcal{P} \mathcal{L} \mathbf{z}(t) + \phi(t, \mathbf{z}_0) + \int_0^t \mathbf{k}(t-s, \mathbf{z}(s)) ds. \quad (34)$$

where $\mathbf{k}(t, \mathbf{z}) := \mathcal{P} \mathcal{L} \phi(t, \mathbf{z}) = \mathcal{P} \mathcal{L} e^{t\mathcal{L}} \mathcal{Q}\mathcal{L}\mathbf{z}$.

Now consider the evolution of $\phi(t, \mathbf{z})$, which is given by

$$\partial_t \phi(t, \mathbf{z}_0) = \mathcal{Q}\mathcal{L}\phi(t, \mathbf{z}_0), \quad (35)$$

with initial condition $\phi(0, \mathbf{z}_0) = \mathcal{Q}\mathcal{L}\mathbf{z}_0 = \mathcal{L}\mathbf{z}_0 - \mathcal{P}\mathcal{L}\mathbf{z}_0 = \bar{\mathbf{f}}(\mathbf{x}_0, \mathbf{e}_0) - \bar{\mathbf{f}}(\mathbf{x}_0, \mathbf{0}) = \mathbf{0}$ since $\mathbf{e}_0 = \mathbf{0}$. Applying \mathcal{P} on both sides of (35) yields

$$\partial_t \mathcal{P}\phi(t, \mathbf{z}_0) = \mathcal{P}\mathcal{Q}\mathcal{L}\phi(t, \mathbf{z}_0) = \mathbf{0},$$

with initial $\mathcal{P}\phi(0, \mathbf{z}_0) = \mathbf{0}$. This implies that $\mathcal{P}\phi(t, \mathbf{z}_0) = \mathbf{0}$ for all t . Hence, applying \mathcal{P} to both sides of (33) yields

$$\frac{\partial}{\partial t} \mathcal{P}\mathbf{z}(t) = \frac{\partial}{\partial t} \mathcal{P} e^{t\mathcal{L}} \mathbf{z}_0 = \mathcal{P} \mathcal{L} \mathbf{z}(t) + \int_0^t \mathcal{P} \mathbf{k}(t-s, \mathbf{z}(s)) ds \quad (36)$$

Restricting to the first n components, $\mathcal{P}\mathbf{z}(t)$ reduces to $\mathbf{x}(t)$ and $\mathcal{P}\mathbf{k}(t-s, \mathbf{z}(s))$ reduces to $\mathbf{k}(t-s, \mathbf{x}(s))$. Recalling that $\mathcal{P}\mathcal{L}\mathbf{z}(t) = \mathcal{P}\bar{\mathbf{f}}(\mathbf{z}(t)) = \bar{\mathbf{f}}(\mathbf{x}(t), \mathbf{0}) = \mathbf{f}(\mathbf{x}(t))$ completes the proof. \square

A.3 Proof of Theorem 3

Proof of Theorem 3. From the definition of $\mathbf{h}(t)$ in (37), we obtain

$$\mathbf{h} = \int_0^t \mathbf{K}(t-s; \mathbf{w}) \mathbf{x}(s) ds = \int_{-\infty}^t \mathbf{K}(t-s; \mathbf{w}) \mathbf{x}(s) ds = \int_0^\infty \mathbf{K}(s; \mathbf{w}) \mathbf{x}(t-s) ds \quad (37)$$

where we used the fact that $\mathbf{x}(t) = 0$ for $t < 0$. Taking derivative on both sides of (37) yields

$$\begin{aligned} \mathbf{h}' &= \int_0^\infty \mathbf{K}(s; \mathbf{w}) \mathbf{x}'(t-s) ds = \int_0^\infty \mathbf{K}(s; \mathbf{w}) \tilde{\mathbf{f}}(\mathbf{x}(t-s), \mathbf{h}(t-s); \mathbf{A}, \boldsymbol{\eta}) ds \\ &= \int_{-\infty}^t \mathbf{K}(t-s; \mathbf{w}) \tilde{\mathbf{f}}(\mathbf{x}(s), \mathbf{h}(s); \mathbf{A}, \boldsymbol{\eta}) ds = \int_0^t \mathbf{K}(t-s; \mathbf{w}) \tilde{\mathbf{f}}(\mathbf{x}(s), \mathbf{h}(s); \mathbf{A}, \boldsymbol{\eta}) ds \end{aligned}$$

where we used the fact that $\mathbf{x}'(t) = \tilde{\mathbf{f}}(\mathbf{x}(t), \mathbf{h}(t); \mathbf{A}, \boldsymbol{\eta}) = 0$ for $t < 0$ in the last equality.

If $\mathbf{K}(t; \mathbf{w}) = \sum_l \mathbf{B}_l e^{-\mathbf{C}_l t}$, then we can take derivative of (37) and obtain

$$\begin{aligned} \mathbf{h}'(t) &= \sum_{l=1}^L \frac{d}{dt} \left(\int_{-\infty}^t \mathbf{B}_l e^{-\mathbf{C}_l t} \mathbf{x}(s) ds \right) = \sum_{l=1}^L \left(\mathbf{B}_l \mathbf{x}(t) - \int_{-\infty}^t \mathbf{B}_l \mathbf{C}_l e^{-\mathbf{C}_l t} \mathbf{x}(s) ds \right) \\ &= \sum_{l=1}^L \left(\mathbf{B}_l \mathbf{x}(t) - \mathbf{C}_l \int_{-\infty}^t \mathbf{B}_l e^{-\mathbf{C}_l t} \mathbf{x}(s) ds \right) = \sum_{l=1}^L (\mathbf{B}_l \mathbf{x}(t) - \mathbf{C}_l \mathbf{h}(t)). \end{aligned}$$

Time discretization (14) can then be obtained by finite difference in time with normalized step size 1 and proper scaling of the network parameters $\boldsymbol{\theta}$. \square

A.4 Proof of Theorem 4

The problem of optimal control has been well studied in both continuous and discrete cases in the past decades [3]. In particular, the discrete optimal control with nonlinear difference equation and the associated maximum principle are exploited. Recently, [37] proposed an optimal control viewpoint of deep learning—the network parameters of a neural network play the role of control variable in a discretized differential equation, and the training of these parameters for the network output to minimize the loss function can be viewed as finding the optimal control to minimize the objective function at the terminal state.

The Pontryagin's Maximum Principle (PMP) provides an important optimality condition of the optimal control problem. In standard optimal control, the control variable can be chosen freely in the allowed set at any given time t , which is a key in the proof of PMP. However, the NMF dynamics derived in (36) and our neural network approximation (10) require a time invariant control $\boldsymbol{\theta}$ throughout. This is necessary since $\boldsymbol{\theta}$ corresponds to the network parameter and needs to be shared across different layers of the RNN, either from the linear kernel case with state $[\mathbf{x}; \mathbf{h}]$ in (14) or the general case with state \mathbf{m} in (16). Therefore, we need to modify the original PMP and the optimality condition for our NMF formulation. To this end, we consider the *total Hamiltonian* of $(\mathbf{m}, \mathbf{p}) := \{(\mathbf{m}_t, \mathbf{p}_t) : 0 \leq t \leq T\}$:

$$\sum_{t=0}^{T-1} H(\mathbf{m}_t, \mathbf{p}_{t+1}; \boldsymbol{\theta}), \quad (38)$$

where $H(\mathbf{m}, \mathbf{p}; \boldsymbol{\theta}) = \mathbf{p} \cdot \mathbf{g}(\mathbf{m}; \boldsymbol{\theta}) - \frac{1}{T} r(\boldsymbol{\theta})$ is the standard Hamiltonian defined in (19). Now we are ready to prove Theorem 4.

Proof of Theorem 4. We consider the augmented state $\boldsymbol{\xi}$ and nonlinear dynamics $\bar{\mathbf{g}}(\cdot; \boldsymbol{\theta})$ associated with \mathbf{m} and $\mathbf{g}(\cdot; \boldsymbol{\theta})$, defined as follows:

$$\boldsymbol{\xi}_0 = \begin{bmatrix} \mathbf{m}_0 \\ \mathbf{0} \\ \vdots \\ \mathbf{0} \end{bmatrix}, \quad \boldsymbol{\xi}_1 = \bar{\mathbf{g}}(\boldsymbol{\xi}_0; \boldsymbol{\theta}) := \begin{bmatrix} \mathbf{g}^1(\mathbf{m}_0; \boldsymbol{\theta}) \\ \mathbf{g}^2(\mathbf{m}_0; \boldsymbol{\theta}) \\ \vdots \\ \mathbf{g}^T(\mathbf{m}_0; \boldsymbol{\theta}) \end{bmatrix} = \begin{bmatrix} \mathbf{m}_1 \\ \mathbf{m}_2 \\ \vdots \\ \mathbf{m}_T \end{bmatrix}, \quad (39)$$

where \mathbf{g}^t stands for the composition of $\mathbf{g}(\cdot; \boldsymbol{\theta})$ for t times.

Without overloading the notations, we reuse \mathcal{J} and ℓ of the objective function (18a) and loss function (17) of \mathbf{m} respectively for the augmented state $\boldsymbol{\xi}$. In addition, following [37], we further simplify the notation by combining the K training data into a single variable $\hat{\mathbf{x}} := [\hat{\mathbf{x}}^{(1)}, \dots, \hat{\mathbf{x}}^{(K)}]$; similar for the state variable \mathbf{x} . In this case, the dynamics \mathbf{g} is applied to each column of \mathbf{x} , and the loss function ℓ is to be interpreted as the average loss as in (17). Furthermore, we temporarily assume the regularization $r(\boldsymbol{\theta}) = 0$ as it is simple to append $\boldsymbol{\theta}$ to the state $\boldsymbol{\xi}$ and merge $r(\boldsymbol{\theta})$ into the loss function $\ell(\boldsymbol{\xi}, \hat{\boldsymbol{\xi}})$. Then the optimal control problem (18) is rewritten as

$$\min_{\boldsymbol{\theta}} \quad \mathcal{J}(\boldsymbol{\theta}) := \ell(\boldsymbol{\xi}, \hat{\boldsymbol{\xi}}) + r(\boldsymbol{\theta}) \quad (40a)$$

$$\text{s.t.} \quad \boldsymbol{\xi}_1 = \bar{\mathbf{g}}(\boldsymbol{\xi}_0; \boldsymbol{\theta}), \quad \boldsymbol{\xi}_0 = [\mathbf{m}_0; \mathbf{0}; \dots; \mathbf{0}]. \quad (40b)$$

Note that (40) is a one-step optimal control with $\bar{\mathbf{g}}(\cdot; \boldsymbol{\theta})$. Now by the discrete Pontryagin's Maximum Principle [3], for the state $\boldsymbol{\xi}^*$ optimally controlled by $\boldsymbol{\theta}^*$, there exists a co-state $\boldsymbol{\psi}^*$, such that $\boldsymbol{\xi}^*$ and $\boldsymbol{\psi}^*$ satisfy the following forward and backward equations for $\boldsymbol{\theta} = \boldsymbol{\theta}^*$:

$$\boldsymbol{\xi}_1^* = \bar{\mathbf{g}}(\boldsymbol{\xi}_0^*; \boldsymbol{\theta}^*), \quad \boldsymbol{\xi}_0^* = [\mathbf{m}_0; \mathbf{0}; \dots; \mathbf{0}], \quad (41a)$$

$$\boldsymbol{\psi}_0^* = \boldsymbol{\psi}_1^* \cdot \nabla_{\boldsymbol{\xi}} \bar{\mathbf{g}}(\boldsymbol{\xi}_1^*; \boldsymbol{\theta}^*), \quad \boldsymbol{\psi}_1^* = -\nabla_{\boldsymbol{\xi}} \ell(\boldsymbol{\xi}_1^*, \hat{\boldsymbol{\xi}}), \quad (41b)$$

where

$$\boldsymbol{\xi}_1^* = [\mathbf{m}_1^*; \dots; \mathbf{m}_T^*] \quad \text{and} \quad \boldsymbol{\psi}_1^* = [\partial_{\mathbf{m}_1} \ell(\boldsymbol{\xi}_1^*, \hat{\boldsymbol{\xi}}); \dots; \partial_{\mathbf{m}_T} \ell(\boldsymbol{\xi}_1^*, \hat{\boldsymbol{\xi}})] = [\mathbf{p}_1^*; \dots; \mathbf{p}_T^*]. \quad (42)$$

In addition, $\boldsymbol{\theta}^*$ maximizes the Hamiltonian \mathcal{H} associated with (41):

$$\mathcal{H}(\boldsymbol{\xi}^*, \boldsymbol{\psi}^*; \boldsymbol{\theta}^*) \geq \mathcal{H}(\boldsymbol{\xi}^*, \boldsymbol{\psi}^*; \boldsymbol{\theta}), \quad \forall \boldsymbol{\theta}, \quad \text{where} \quad \mathcal{H}(\boldsymbol{\xi}, \boldsymbol{\psi}; \boldsymbol{\theta}) := \boldsymbol{\psi}_1 \cdot \bar{\mathbf{g}}(\boldsymbol{\xi}_0; \boldsymbol{\theta}) - r(\boldsymbol{\theta}). \quad (43)$$

Combining (42), (43), and the definition of H in (19) yields the maximization of total Hamiltonian at the optimal control $\boldsymbol{\theta}^*$:

$$\sum_{t=0}^{T-1} H(\mathbf{m}_t^*, \mathbf{p}_{t+1}^*; \boldsymbol{\theta}^*) \geq \sum_{t=0}^{T-1} H(\mathbf{m}_t^*, \mathbf{p}_{t+1}^*; \boldsymbol{\theta}), \quad \forall \boldsymbol{\theta}.$$

For any control $\boldsymbol{\theta}$ and its state and co-state variables $\boldsymbol{\xi}^\theta$ and $\boldsymbol{\psi}^\theta$ following (41) with $\boldsymbol{\theta}$ (also corresponding to \mathbf{m}_t^θ and \mathbf{p}_t^θ for $t = 0, \dots, T$), we have

$$\begin{aligned} \nabla_{\boldsymbol{\theta}} \mathcal{J}(\boldsymbol{\theta}) &= \nabla_{\boldsymbol{\xi}} \ell(\boldsymbol{\xi}_1^\theta, \hat{\boldsymbol{\xi}}) \cdot \nabla_{\boldsymbol{\theta}} \boldsymbol{\xi}_1^\theta + \nabla_{\boldsymbol{\theta}} r(\boldsymbol{\theta}) \\ &= [\partial_{\mathbf{m}_1} \ell(\boldsymbol{\xi}_1^\theta, \hat{\boldsymbol{\xi}}); \dots; \partial_{\mathbf{m}_T} \ell(\boldsymbol{\xi}_1^\theta, \hat{\boldsymbol{\xi}})] \cdot [\partial_{\boldsymbol{\theta}} \mathbf{g}(\mathbf{m}_0^\theta; \boldsymbol{\theta}); \dots; \partial_{\boldsymbol{\theta}} \mathbf{g}(\mathbf{m}_{T-1}^\theta; \boldsymbol{\theta})] + \nabla_{\boldsymbol{\theta}} r(\boldsymbol{\theta}) \\ &= -\sum_{t=1}^T \left(\mathbf{p}_t^\theta \cdot \partial_{\boldsymbol{\theta}} \mathbf{g}(\mathbf{m}_t^\theta; \boldsymbol{\theta}) + \frac{1}{T} \nabla_{\boldsymbol{\theta}} r(\boldsymbol{\theta}) \right) \\ &= -\sum_{t=1}^T \partial_{\boldsymbol{\theta}} H(\mathbf{m}_t^\theta, \mathbf{p}_{t+1}^\theta; \boldsymbol{\theta}), \end{aligned}$$

which completes the proof. \square

B Discussion

Existing approaches to influence estimation can be approximately classified into two categories: sampling-based methods [8, 11, 17, 27, 42, 49] and analytical methods [13, 18, 25, 29, 31, 39, 40, 41, 62, 64, 67]. Sampling-based methods estimate influence by extracting key statistics from generated cascades initiated from the source set. However, the computation complexity to maintain target approximation error grows rapidly with increasing network density and diffusion duration. On the other hand, analytic solutions of influence estimation on general continuous-time diffusion network are known to be NP-hard problems due to the exponentially growing refined state space dimension in network size. Influence estimation are also considered without explicit knowledge of diffusion model, but often have various assumptions on the underlying network structure and additional information for the cascade data [6, 7, 15, 35, 36, 38, 52, 54, 56, 59, 65, 66, 68].

Inference of diffusion networks [2, 44] often considers data generated from continuous-time independent cascade models, and the goal is to recover the network edges [12, 22, 47, 53] or the diffusion model parameters

of the edges [21]. In this case, maximum likelihood estimate can be conducted given the condition intensity for the diffusion model and the training cascades data.

The present work is derived from the analytic formulation of the problem, but reduces the evolution system to the low dimensional resolved space which captures the main drift of the dynamics. The difference between the resolved and refined dynamics are accurately approximated by a deep neural net, which can be efficiently trained by a small amount of training data. The proposed approach also introduces a highly interpretable learning framework, where the network structure and diffusion parameter can be learned jointly with estimation function directly from cascade data.

C Experiment Supplements

Implementation details In our NMF implementation, we use a standard 3-layer LSTM architecture for the RNN ε for each time t . Regularization terms using l_1 -norm of all parameters are added to the loss function to promote their sparsity and robustness. Specifically, we use 0.001 to weight \mathbf{A} and 0.0001 to all other trainable parameters, respectively. The NMF networks are trained and tested in TensorFlow [1] by Adam optimizer with default parameters ($\text{lr}=0.001$, $\beta_1=0.9$, $\beta_2=0.999$, $\epsilon=1\text{e-}8$) on a Linux workstation with Intel 8-Core Turbo 5GHz CPU, 64GB of memory, and an Nvidia RTX 2080Ti GPU. The LSTM model is trained and tested in the same setting as NMF except a fixed regularization weight 0.001 for all trainable parameters. InfluLearner is trained in Matlab, and the number of features is set to 128. All experiments are performed on the same machine. Given ground truth node infection probability \mathbf{x}^* , the Mean Absolute Error (MAE) of influence (Inf) and infection probability (Prob) of estimated \mathbf{x} are defined by $|\mathbf{1} \cdot (\mathbf{x}_t - \mathbf{x}_t^*)|$ and $\|\mathbf{x}_t - \mathbf{x}_t^*\|_1/n$ for every t , respectively.

Inference of Node Interdependencies Due to its highly interpretable structure, NMF can also learn the node inter-dependencies through \mathbf{A} . In addition to the quantitative evaluations provided in Section 4, we show the visual appearance of \mathbf{A} inferred by NMF in Figure 3. The ground truth \mathbf{A}^* and \mathbf{A} inferred by NETRATE are also provided for comparison. As we can see, \mathbf{A} inferred by NMF is much more faithful to \mathbf{A}^* than that by NETRATE. Note that NETRATE requires knowledge of specific diffusion model type (Rayleigh in this test) whereas NMF does not. This result shows that NMF is versatile and robust when only cascade data are available.

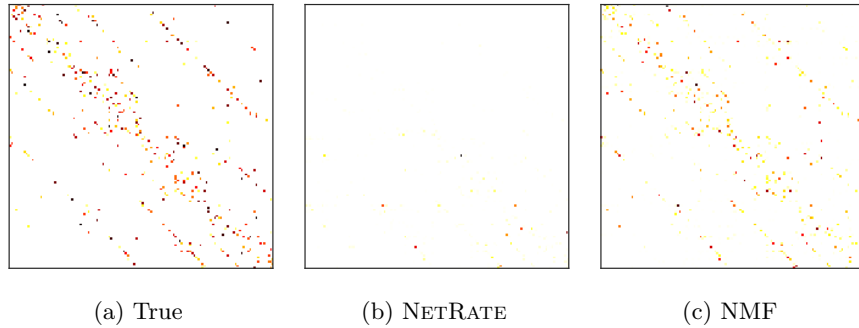


Figure 3: Ground truth \mathbf{A}^* (left) and \mathbf{A} inferred NETRATE (middle) and NMF (right) under the same color scale using cascaded data from a Hierarchical network with Rayleigh diffusion model.

Performance with different network sizes We test NMF on increasing network size up to $n = 2048$ with $|\mathcal{E}| = 2n$ for each n using Hierarchical network and exponential diffusion model on cascade data containing 10,000 cascades. 100 extra cascades are generated for 20%-validation and 80%-test.

Figure 4 (a)–(b) shows the MAE of influence (Inf) and infection probability (Prob) estimated by NMF versus time for varying n , which indicate that the error remains low relative to network size. Figure 4 (c) shows the run time (in seconds) of training for different network size n , which increases slowly in n . The

batch size of training cascade data is set to 50 for the network with 2048 nodes, and is 100 for smaller networks. The training is terminated when the average MAE of infection probability on validation data does not decrease for 20 epochs.

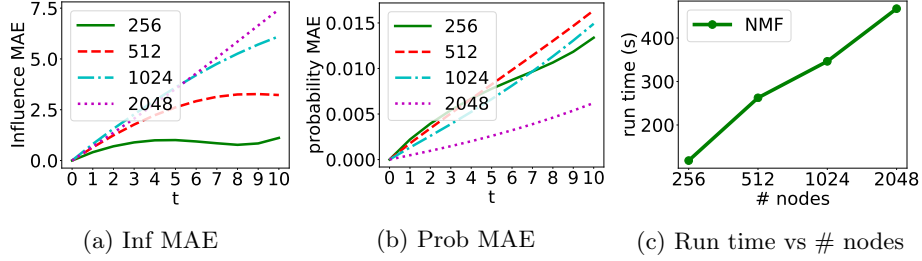


Figure 4: (a)–(b) MAE of influence (Inf) and infection probability (Prob) estimated by NMF for Hierarchical networks with increasing network sizes from 256 to 2048. (c) Run time (in seconds) for training versus network sizes.

Additional results of infection probability estimation We test a total of 9 combinations of network structures and diffusion models. Specifically, we generate Hierarchical (Hier), Core-periphery (Core), and Random (Rand) networks, and use Exponential (Exp), Rayleigh (Ray) and Weibull (Wbl) diffusion models on each of these networks. All diffusion parameters are drawn from $\text{Unif}[1,10]$. Here we stretch NMF and apply to Weibull diffusion model even it has two parameters for each edge. The experiment setting and evaluation metrics are the same as in Section 4. The MAE of influence and node infection probabilities are shown in Figure 5, which shows that NMF consistently performs well with low estimation error after trained by cascade data. Again, it is worth noting that InflLearner requires the identity of source node for every infection in the entire cascade during training, which is generally not available in practice nor needed in NMF.

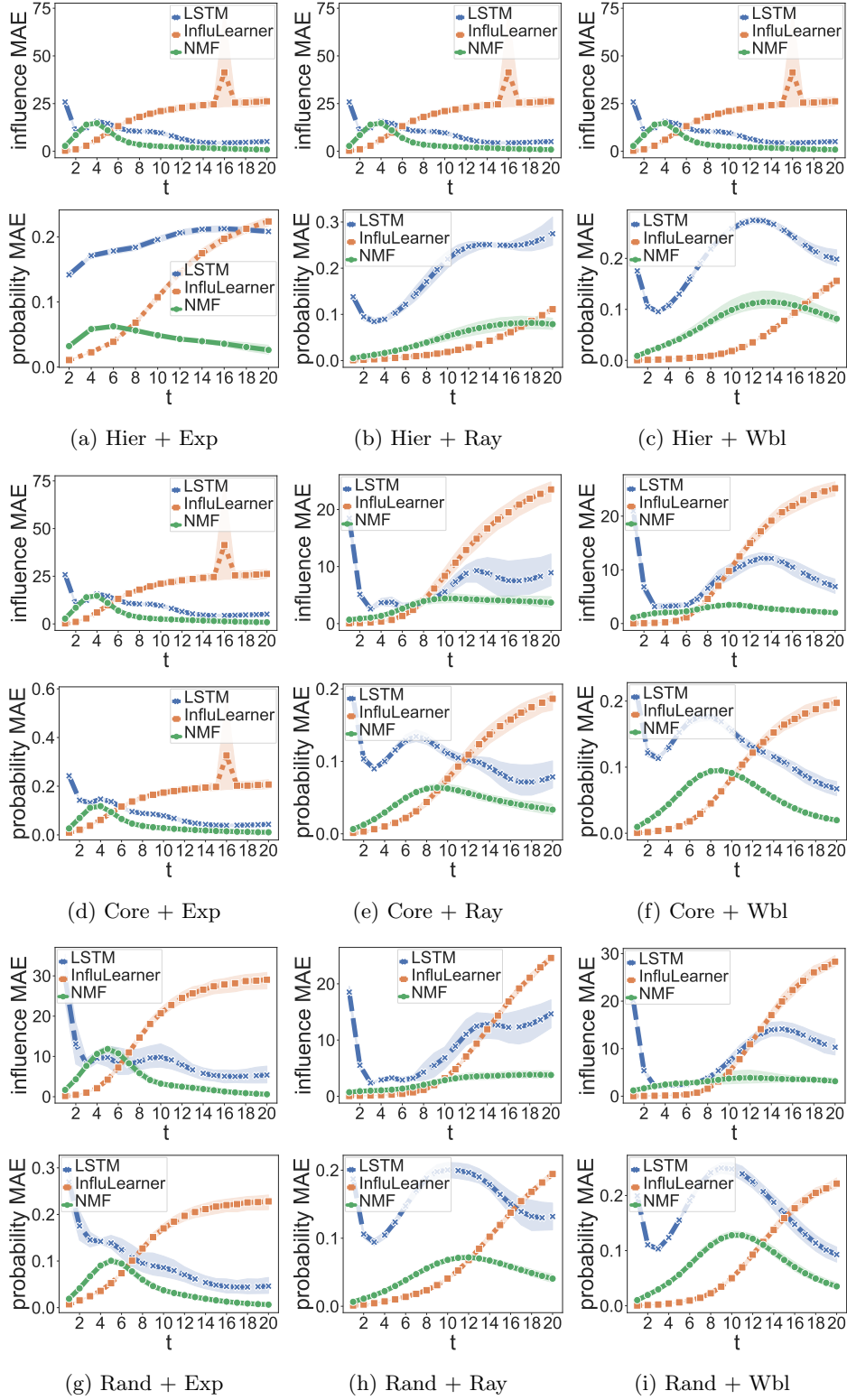


Figure 5: MAE of influence (top) and node infection probability (bottom) by LSTM, InfluenzaLearner, and NMF on each of the 9 different combinations of Hierarchical (Hier), Core-periphery (Core) and Random (Rand) networks, and exponential (Exp), Rayleigh (Ray) and Weibull (Wbl) diffusion models. Mean (centerline) and standard deviation (shade) over 100 tests are shown.